



Phase transformation, thermal behavior, and magnetic study of new $(\text{FeSiBP})_{100-x}\text{Cu}_x$ glassy alloys obtained by melt-spinning in air

D. Perea-Cabarcas^{1,2,a)} , C. A. Parra Vargas², F. Echeverría Echeverría¹, F. J. Bolívar Osorio¹

¹ Centro de Investigación, Innovación de Desarrollo de Materiales – CIDEMAT, Universidad De Antioquia, Calle 62 N° 52 – 59, P. O. Box 1226, Medellín, Colombia

² Grupo Física de Materiales (GFM), Universidad Pedagógica y Tecnológica de Colombia, Avenida Central Del Norte 39-115 Tunja, 15001 Boyacá, Colombia

^{a)} Address all correspondence to this author. e-mail: darling.perea@udea.edu.co

Received: 31 January 2023; accepted: 11 May 2023

In the current work, a new variation of the FeSiBPCu system with good glass forming ability and soft magnetic properties was developed and investigated. The effect of copper addition on the FeSiBP base alloy was studied in the system $(\text{Fe}_{0.77}\text{Si}_{0.08}\text{B}_{0.1}\text{P}_{0.05})_{100-x}\text{Cu}_x$ with $x = 0, 0.25, 0.5, 0.75$ and 1.0 at%. Microstructural evolution upon the annealing process was evaluated by XRD and TEM, revealing the formation of $\alpha\text{-Fe}(\text{Si})$, Fe_2B and $\text{Fe}_3(\text{B,P})$ crystalline phases. VSM allowed to determine that the combination of chemical composition and microstructure with the best soft magnetic properties after the annealing corresponds with the alloy with 0.75% Cu. In addition, activation energy for glass transition and the first crystallization event were calculated using the Kissinger method. The research findings demonstrated that maintaining the relationship between the main elements, it is possible to keep the good glass forming ability with the possibility of developing a nanocrystalline structure with soft magnetic performance.

Introduction

Since their appearance, amorphous iron-based alloys have aroused considerable interest for various types of electrical and electronic devices, such as sensors, motors, power transformers, and reactors, among others, replacing traditional silicon steels that have relatively inferior magnetic properties, such as high coercivity and high losses, although they have a high saturation magnetization, superior to those of amorphous alloys [1].

The search for amorphous iron-based alloys with better performance, good mechanical properties and magnetic properties superior to silicon steels has attracted attention during the last decades in different sectors of science and technology. This search led to a new generation of magnetically soft materials, which emerged with the discovery of the Finemet alloy [2], with a composition $\text{Fe}_{73.5}\text{Si}_{13.5}\text{B}_9\text{Nb}_3\text{Cu}_1$, whose structure is composed of nanometer-sized grains of the $\alpha\text{-Fe}(\text{Si})$ crystalline phase immersed in a residual amorphous phase after annealing for one hour at 550 °C [2, 3]. In this alloy the grain size did not exceed 20 nm and soft magnetic properties were achieved

that have not been surpassed so far. This type of nanocrystalline alloys is produced by the controlled crystallization of amorphous precursors; they break the classical rules that state that the best soft magnetic properties are obtained with large grain sizes and the adverse effect that crystallization has on the magnetic softness of amorphous alloys [4, 5]. Other nanocrystalline alloys have been developed, including NANOPERM and HITPERM, whose systems are FeZrBCu [6] and FeCoZrBCu [7], respectively. It is well known that the addition of metals such as Nb, Ga, Y and Co significantly improve the glass-forming ability of Fe-Si-B alloys but reduce their soft magnetic properties [8], moreover, these elements are scarce, costly and limit productivity due to the extreme care that must be taken to avoid oxidation. For the above reasons, The FeSiBPCu alloy system has proven to be one of the most studied for its excellent soft magnetic properties, ideal for the study of the mechanism of crystallization and formation of a nanocrystalline phase [9]. As a result of those studies, different alloys were developed in a wide range of compositions in the FeSiBPCu system; of this group of

alloys, the NANOMET alloy with a saturation magnetization of 1.94 T and a coercivity of 10 A/m stands out [8, 10–14]. With the addition of Cu to the FeSiBP system, new alloys were developed with improved mechanical properties [15, 16] and capable of developing a nanocrystalline structure by heat treatment. The presence of Cu and P determine the crystallization behavior of the alloy, Cu atoms act as nucleation site for the α -Fe(Si) phase grains and P stabilizes the amorphous phase by restricting the formation of Fe, B and P crystalline phases, while limiting the growth of α -Fe(Si) phase grains, the resulting structure is composed of nano-sized grains embedded in an amorphous matrix.

Although it is reported that copper in FeSiBP alloys favors crystallization and can lead to obtaining a heteroamorphous structure with bcc iron clusters of about 2–3 nm [17, 18], in this work a method of obtaining FeSiBPCu ribbons by the melt spinning method in air is developed. Under the established conditions, ribbons with completely amorphous structure were obtained in the whole range of compositions. The correlation between composition, thermal stability, annealing temperature and the soft magnetic properties of this nanocrystalline alloy systems is discussed in detail.

Results and discussion

The alloy design was mainly focused on the fact that the alloy should have a good glass-forming ability [19, 20]. The base alloy of the $(\text{Fe}_{0.77}\text{Si}_{0.08}\text{B}_{0.1}\text{P}_{0.05})_{100-x}\text{Cu}_x$ system, which for simplicity will be referred to as $(\text{FeSiBP})_{100-x}\text{Cu}_x$ from this point on, was chosen based on one of the criteria for the formation of an amorphous material, i.e., the proximity to a eutectic point [21]. The Fe-B system exhibits an eutectic at 1448 K (1175 °C) with an iron concentration of 83%, this being a good starting

point to extrapolate the alloy to a multicomponent system. Figure 1a shows the Fe-B phase diagram constructed using FactSage™ 7.1 [22], in this figure it can be seen that silicon and phosphorus addition shifts the Fe-B eutectic towards a concentration of 10% atomic B. The P content was set at 5% because, although it increases the glass-forming capacity of the alloy, above this value it increases the coercivity of the amorphous alloy [23]. Varying the Fe content moves the final composition away from the eutectic point, so an iron content of 77% is set as the concentration that best satisfies the criterion of closeness to a eutectic. Thus, the final composition of the alloy is set as $\text{Fe}_{77}\text{Si}_8\text{B}_{10}\text{P}_5$, indicated by the dotted line. Besides the criterion of proximity to eutectic points, a series of empirical rules, derived from experience and research over decades, have been proposed to design alloys with good glass-forming capacity from the stabilization of the material in the molten state [24]. These rules, developed by Inoue, state the following: the alloy must be multicomponent, with at least 3 alloying elements; the ratio of atomic radii between the alloys and the main element must be greater than 12% and negative heats of mixing between the constituents. In the FeSiBP system the elements Si, B and P have size differences of 14, 39 and 29%, respectively, also characterized by negative mixing heats with iron as illustrated in Fig. 1b [25, 26].

The results of the XRD analysis of the as-spun ribbons are presented in Fig. 2, in it the diffraction patterns of the samples obtained with the different compositions of the $(\text{FeSiBP})_{100-x}\text{Cu}_x$ system can be observed; in all cases patterns typical of amorphous samples were obtained, characterized by having a wide and low intensity hump centered at $2\theta \approx 52^\circ$ indicating the formation of a homogeneous phase without the presence of crystalline phases.

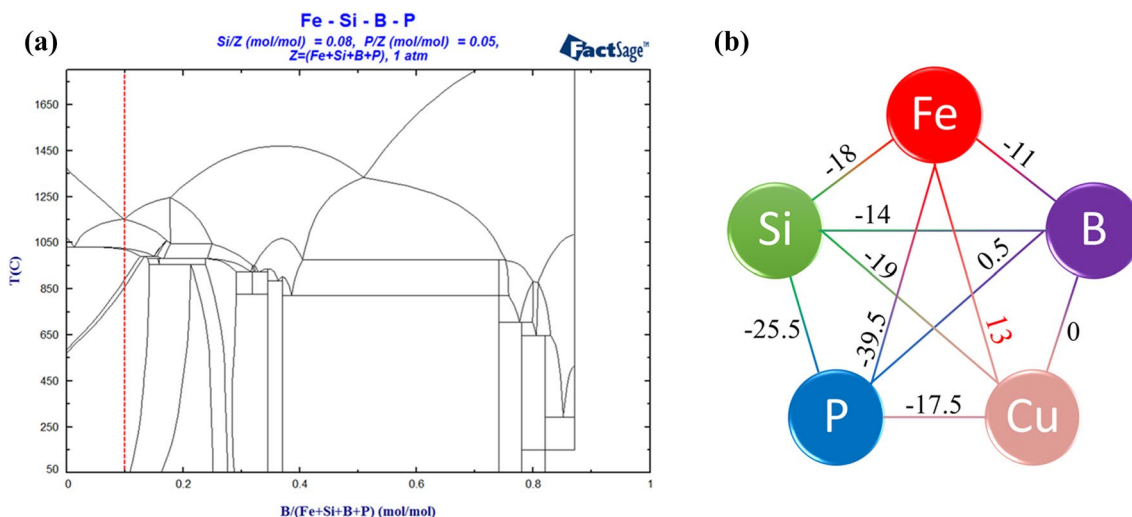


Figure 1: (a) Phase diagram of the base alloy and (b) values of ΔH_{Mix} (kJ/mol) calculated for the atomic pairs of elements that make up the alloy system.

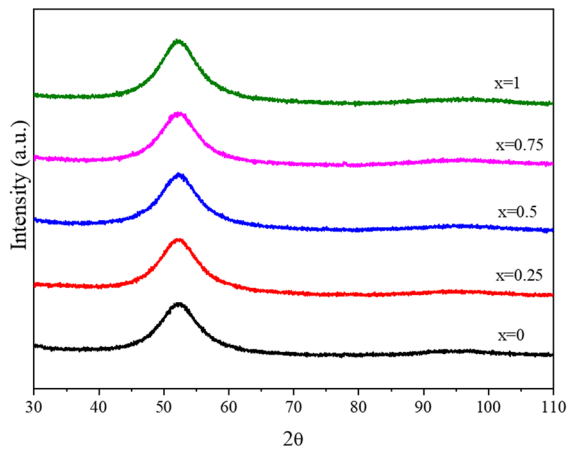


Figure 2: XRD patterns for as-spun (FeSiBP)_{100-x}Cu_x ribbons.

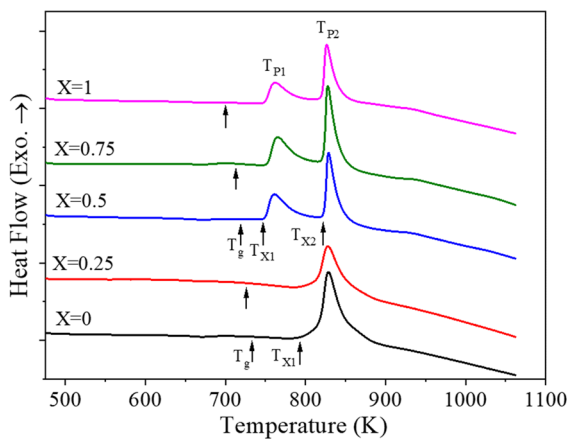


Figure 3: DSC curves for the (FeSiBP)_{100-x}Cu_x ($x=0, 0.25, 0.5, 0.75$ and 1.0) amorphous alloy system at a heating rate of 20 K/min .

The influence of copper on the thermal stability of the base alloy can be evaluated from calorimetric measurements. It is worth mentioning that characteristic temperatures such as the onset exothermic peak of crystallization (T_{x1} and T_{x2}) and the peak temperature (T_{p1} and T_{p2}) are distinguished as the vertical up arrows in the DSC scan shown in Fig. 3. In this figure it can be noticed that in the base alloy there is a single exothermic event characterized by a crystallization peak in which a small shoulder is seen on each side of the main peak, representing

the formation of several crystalline phases simultaneously during heating, where the high entropy amorphous phase is transformed into more stable crystalline phases. The addition of 0.25% Cu does not represent a significant variation in the peak, however, the addition of Cu from 0.5% onwards causes a two-stage crystallization process to occur. In the samples with higher Cu content, two exothermic reactions can be observed in the material, which are represented by two crystallization peaks (T_{x1} and T_{x2}) starting at 747 and 822 K, respectively. As shown in Table 1, increasing the Cu content to 0.75 and 1% does not generate significant changes in the variation of crystallization temperatures. This type of multistage thermal behavior is desirable when precipitation of the primary crystalline phase is desired without the presence of undesirable secondary phases.

Figure 4a shows the diffraction patterns of the base alloy isothermally annealed at different temperatures. The samples annealed at 723 and 763 K continue with their amorphous character, while at 798 and 828 K a small, crystallized fraction corresponding to the α -Fe phase begins to be observed. At 973 K the complete crystallization of the material can be appreciated, with a mixture of three crystalline phases, α -Fe(Si), Fe_2B and $\text{Fe}_3(\text{B,P})$, which are formed in a single crystallization event. The phase mixture is dominated by the α -Fe(Si) phase, which exhibits a slight shift to higher 2θ values with increasing annealing temperature due to the diffusion of Si atoms into the bcc α -Fe crystal lattice, forming a solid solution. The lattice parameter of the α -Fe(Si) phase identified in the XRD analysis (ICSD 98-015-9353) is 2.8420 \AA while that of pure α -Fe is 2.8660 \AA , evidencing how the increase of the content of the small Si atom in the α -Fe(Si) phase reduces the lattice parameter a_0 .

The patterns obtained in the XRD analysis of the alloys with small additions of Cu and annealed are shown in Fig. 4b–e. In Fig. 4b where the patterns belonging to the sample with 0.25% Cu are observed, it can be seen that at 798 K a small amount of the α -Fe(Si) phase begins to crystallize; the increase in annealing temperature causes other secondary phases to precipitate, mainly composed of different iron borides. With annealing at 828 K the Fe_3B phase is formed, which at higher annealing temperatures will transform to more stable phases such as Fe_2B and $\text{Fe}_3(\text{B,P})$ [27, 28]. This crystallization mechanism occurs in several stages in a narrow temperature range as in the base alloy because like the latter,

TABLE 1: Characteristic temperatures (K) of the as-spun ribbons of the (FeSiBP)_{100-x}Cu_x amorphous alloys system.

Alloy	T_g	T_{x1}	T_{p1}	T_{x2}	T_{p2}	ΔT_x
Base— $\text{Fe}_{77}\text{Si}_8\text{B}_{10}\text{P}_5$	733	793	828	–	–	60
(FeSiBP) _{99.75} Cu _{0.25}	726	788	826	–	–	62
(FeSiBP) _{99.5} Cu _{0.5}	719	747	760	822	828	28
(FeSiBP) _{99.25} Cu _{0.75}	713	748	765	817	827	34
(FeSiBP) ₉₉ Cu ₁	700	748	761	817	826	48

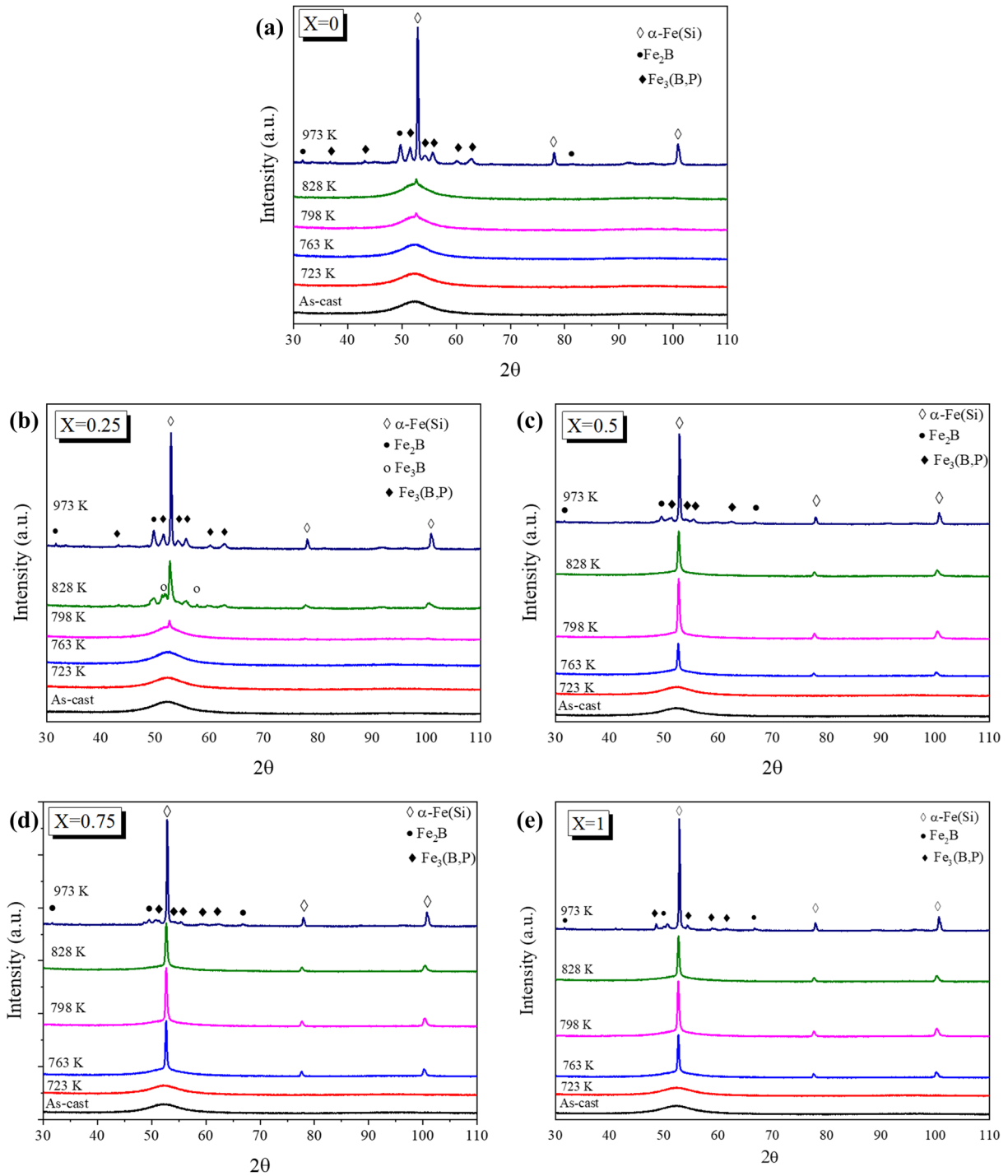


Figure 4: Diffraction patterns of $(\text{FeSiBP})_{100-x}\text{Cu}_x$ system alloys annealed at different temperatures. (a) $x=0$, (b) $x=0.25$, (c) $x=0.5$, (d) $x=0.75$ and (e) $x=1.0$.

the sample with 0.25% Cu presents only one crystallization event in the DSC analysis. It is evident that copper facilitates the initial precipitation of the α -Fe phase because as observed in Fig. 3, there is a reduction in T_{x1} and an incipient separation at the crystallization peak.

The samples with 0.5, 0.75 and 1% copper exhibit a similar behavior towards annealing as shown in Fig. 4c-e. In all of them it can be observed at 763 K the beginning of the crystallization of the α -Fe(Si) phase, as the annealing temperature increases this peak becomes higher evidencing the progress of

the crystallization process and slightly shifts towards higher values at 2θ . This shift, as mentioned above, is due to the diffusion of silicon atoms within the iron crystal lattice. Finally, in the curve corresponding to the annealing at 973 K, it is possible to observe the secondary phases Fe_2B and $Fe_3(B,P)$ that are formed during the second stage of crystallization.

The TGA analysis in the presence of a magnetic field shows the dependence of the magnetization on temperature. The result of this analysis is presented in Fig. 5, where it can be observed that with increasing temperature the magnetization decreases until reaching the Curie temperature, that is, the temperature where the amorphous phase reaches its paramagnetic state. As can be seen in the same figure, the Curie temperature is approximately 673 K for all alloys. Heating above this temperature causes the curves to establish zones where there is an increase in mass, i.e., an increase in the magnetization of the material. The first crystallization peak observed in the DSC associated with the α -Fe(Si) phase is found at 747 K, which explains why at temperature Tx1 in the TGA analysis curve the alloys with

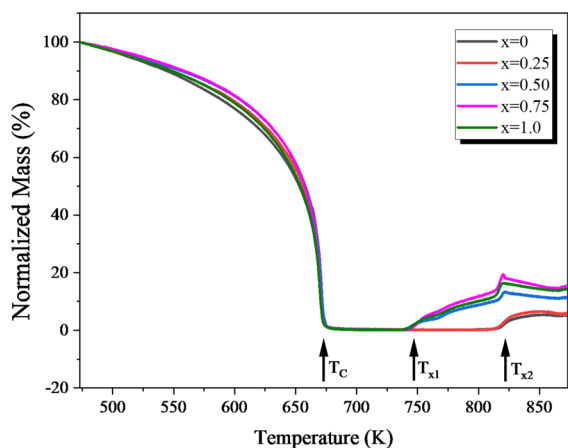
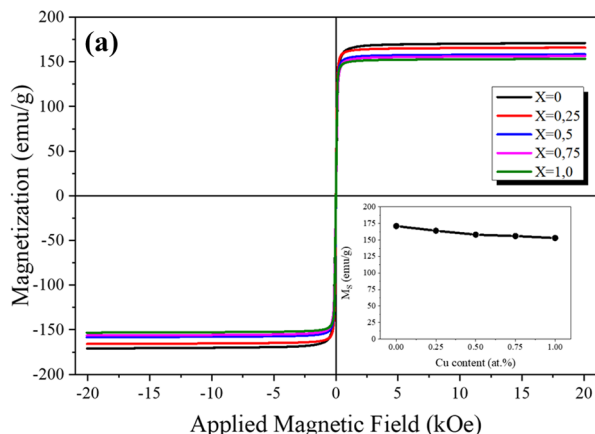


Figure 5: TGA measurements for all samples at a heating rate of 10 K/min.



higher Cu content (0.5, 0.75 and 1% at.) present an increase in their mass, it is also observed that the higher the content of the fraction of crystallized α -Fe(Si), the higher its mass. Similarly, a change in the mass of all the alloys is observed at a temperature close to 820 K; this change coincides with the onset of crystallization of the base alloy, the alloy with 0.25% Cu and the second stage of crystallization in the alloys with 0.5, 0.75 and 1% Cu i.e., Tx2.

The hysteresis loops obtained in the VSM analysis are presented in Fig. 6. In Fig. 6a it can be observed that the sample with the highest saturation magnetization corresponds to the base alloy with 171 emu/g; this Ms value reduces as a function of the Cu addition, reaching a value of 153 emu/g with the addition of 1% Cu. It should be noted that the inset in the graph of Fig. 5a presents a smooth change of slope when the Cu content reaches 0.5%, becoming less steep. This result is in agreement with that observed in the thermal analysis, where the addition of Cu between 0.5 and 1% stabilizes the amorphous phase.

Figure 6b displays the VSM results of the alloys annealed at 798 K. In the hysteresis loops, a behavior similar to that of the as-spun samples can be observed, where Ms decrease with increasing Cu content, until its concentration reaches a value of 0.5%. Nevertheless, with the increase of Cu content to 0.75%, a considerable increase in Ms is obtained, reaching a value of 177 emu/g, which is higher than that of the base alloy. This behavior is due to the structure of the material annealed at 798 K; it has been shown that an amorphous precursor with a large temperature interval between two crystallization peaks can be transformed into a nanocrystalline structure with a large magnetocrystalline anisotropy by annealing at an intermediate temperature between the two peaks. [18].

The magnetic behavior of the annealed samples can be attributed to the microstructure obtained in both alloys. Figure 7 shows the TEM analysis of the base alloy and the 0.75% Cu sample with their respective SAED patterns. Figure 7a–c

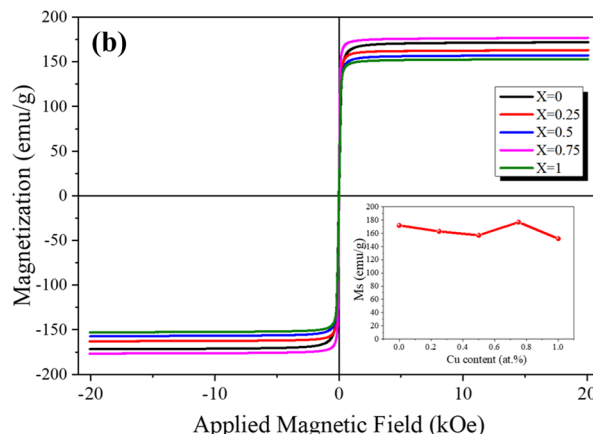


Figure 6: (a) Hysteresis loops for amorphous alloys, (b) Hysteresis loops for samples annealed at 798 K.

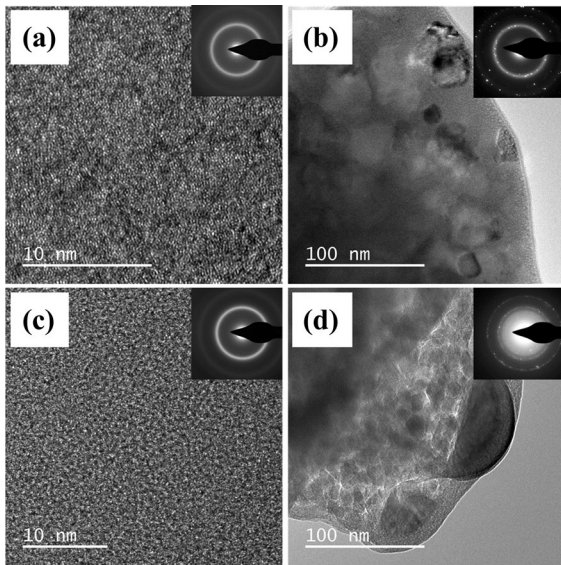


Figure 7: The TEM results related to (a) As-spun base alloy, (b) base alloy annealed at 798 K, (c) as-spun (FeSiBP)_{99.25}Cu_{0.75} and (d) (FeSiBP)_{99.25}Cu_{0.75} annealed at 798 K.

exhibit pepper-salt type images typical of an amorphous state. In addition, SAED patterns corroborates that there are no extra diffraction spots which confirms that the obtained samples are consistent with a glassy structure. In these figures it can be seen how, by annealing the ribbons at 798 K, structures with grains of different morphology and size embedded in a remanent amorphous matrix are developed. While in the base alloy grains with a wide size distribution can be found, some of them reaching 60 nm, in the sample with 0.75% Cu there is a narrow size distribution, with an average size of 27.6 nm calculated according to the Scherrer equation from the XRD data. In both alloys the combined effect of B and P limits the excessive growth of the grains, however, the presence of Cu favors heterogeneous nucleation, thus generating a large number of nucleation sites which, added to the inhibitory effect of the remaining amorphous phase and the intermediate layer rich in the metalloid elements B and P results in the refinement of the structure. This structure of nanometer grains composed of the α -Fe(Si) phase is responsible for the soft magnetic properties of this type of alloys. The insets in Fig. 7b and 7d correspond to the SAED patterns in the micrographs. In Fig. 6b a ring describing the remanent

amorphous phase is observed, in this one a series of dots are found corresponding to the planes of the α -Fe(Si) phase. The dots observed around the ring are equivalent to the Fe₂B and Fe₃(B,P) phases that precipitate simultaneously with the α -Fe(Si) phase in the single crystallization event present in the base alloy. The SAED pattern in Fig. 7d is characterized by the disappearance of the halo observed in Fig. 7c and the appearance of two rings formed by multiple dots revealing only the presence of the nanocrystalline α -Fe(Si) phase.

The overall activation energy for a thermal event such as the crystallization of an amorphous alloy under constant heating rate conditions can be calculated using Kissinger's method [29–31], which relates the temperature dependence to the heating rate β through the following equation:

$$\ln \frac{\beta}{T^2} = -\frac{E}{RT} + \text{Const.} \quad (1)$$

where β is the heating rate, R is the ideal gas constant and T is the temperature of the evaluated event. By plotting $-\ln(\beta/T^2)$ vs. $1/T$, a straight line is obtained, and the value of the activation energy for a characteristic event can be calculated using the slope ($m = E/R$).

Table 2 summarizes the characteristic values of the thermal events observed in the alloys with $x=0$ and 0.75%Cu at different heating rates. As can be realized, these events are thermally triggered and are dependent on the heating rate, leading to a shift to higher temperatures while the heating rate is increased from 5 to 40 K/s. In this table.

The plots of $-\ln(\beta/T^2)$ vs. $1/T$ used in the calculation of the activation energies are shown in Fig. 8 and the results of this analysis are presented in Table 2. During heating, the atoms of the amorphous alloy overcome the energy barrier required to form clusters of atoms that will lead to the formation of the various crystalline phases present in the equilibrium [29, 32]. In this analysis, a slight increase in E_g is evidenced with the addition of Cu, revealing that Cu stabilizes the amorphous phase, on the other hand, the addition of 0.75% Cu to the base alloy reduces by 37% the crystallization activation energy, i.e., it reduces the energy required to overcome the thermal barrier and reconstruct the atomic configuration of the atoms of the α -Fe phase. In addition, it improves the thermal stability of the residual amorphous phase against crystallization, as a more far-reaching

TABLE 2: Glass transition temperature (T_g), onset of crystallization (T_{x1}), first crystallization peak (T_{p1}) for the (FeSiBP)_{100-x}Cu_x system alloys with $x=0$ and $x=0.75$ at different heating rates and activation energy according to Kissinger's method.

x	5 K/min		10 K/min		20 K/min		40 K/min		Activation energy (kJ/mol)		
	0	0.75	0	0.75	0	0.75	0	0.75	0	0.75	
T_g	–	–	717	692	733	711	760	730	E_g	133	141
T_x	781	731	783	739	793	748	798	758	E_x	543	341
T_{p1}	810	742	819	752	828	764	839	776	E_p	393	278

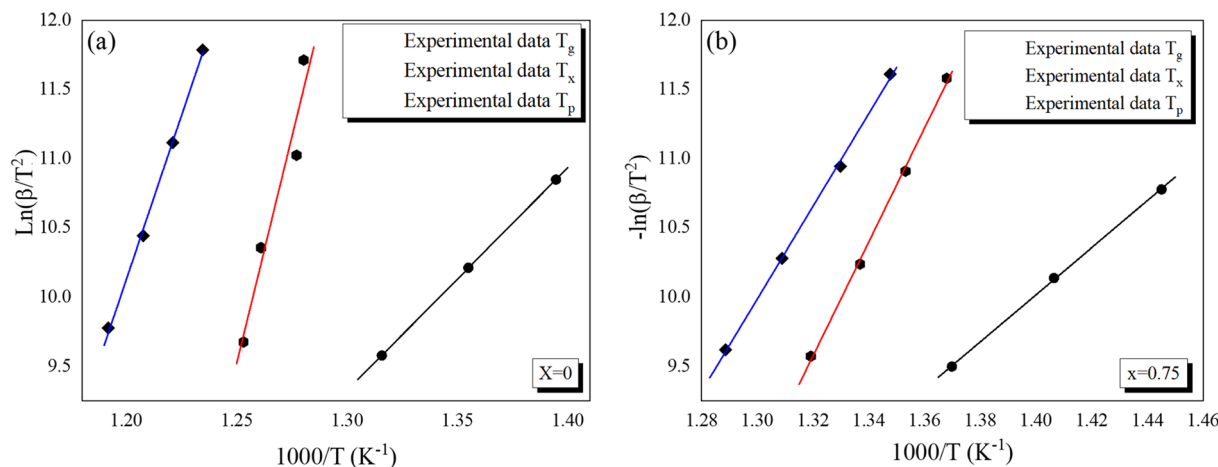


Figure 8: Kissinger plots to calculate the activation energies E_g , E_x and E_p for (a) the base alloy and (b) the 0.75%Cu alloy.

rearrangement of atoms is required to form the structure of the $Fe_3(B,P)$ and Fe_2B phases. [33].

Conclusions

The effect of copper addition on glass forming ability, thermal properties, crystallization, and magnetic behavior of $Fe_{0.77}Si_{0.08}B_{0.1}P_{0.05}$ base alloy was studied by several analytical techniques. According to the obtained results, the following conclusions can be made:

In spite of the fact that copper favors crystallization, DSC, XRD and TEM analyses showed that it is possible to obtain completely amorphous alloys, with good glass-forming ability in the whole range of compositions while maintaining the proportion of the base alloy elements.

The findings revealed that the α -Fe(Si), Fe_2B and $Fe_3(B,P)$ are simultaneously formed during the decomposition of the amorphous phase in the base alloy. Nevertheless, the addition of copper starting at 0.5% encourages the crystallization of the α -Fe(Si) phase in a first independent thermal event.

Compared to Cu-free alloys, the GFA for Cu-containing alloys is unimproved. This reduction in GFA is compensated by obtaining alloys with tunable soft magnetic properties by controlled crystallization of nanometer-sized grains of the α -Fe(Si) phase through heat treatment, with potential application in the fabrication of soft magnetic cores.

Materials and methods

Master alloy ingots with nominal compositions of $(Fe_{0.77}Si_{0.08}B_{0.1}P_{0.05})_{100-x}Cu_x$, with $x = 0, 0.25, 0.5, 0.75, 0.75$ and 1 at. %, were prepared by induction melting in a vacuum chamber under argon atmosphere, starting from stoichiometric mixtures of Fe (Aldrich Chemistry— $\geq 99\%$), Si (Aldrich

Chemistry—99%), FeB (American Elements—99%), Fe_2P (Alfa Chemistry—99%) and Cu powders. Each ingot was melted three times to ensure chemical homogeneity. Ribbons were then prepared by using a homemade single-roller melt-spinning in air at atmospheric pressure conditions. Argon was used as ejection gas with an overpressure of 200 mbar, the wheel speed was 35 m/s, the gap between the wheel and crucible was 400 μm , and the ejection temperature employed was 1480 K. Ribbons about 1.2 mm wide and 22 – 35 μm thick were obtained.

The structural characterization of the as-spun and annealed ribbons was carried out by X-ray diffraction (XRD) using a PANalytical X'pert Pro diffraction system with $Co-K\alpha$ ($\lambda = 1.789010$) radiation. Differential Scanning Calorimetry (DSC) was employed to evaluate the thermal behavior of the as-spun ribbons in a TA Instruments Q600 thermal analyzer. The glass transition temperature (T_g) was measured using the TA Instruments Universal Analysis 2000 software. In the curves obtained by DSC T_g it is not easily visible, however, by means of the software it is possible to zoom in and using the tool to examine T_g a temperature range can be established in which it detects the inflection point where the glass transition occurs. Thermomagnetic Analysis (TMA) was used to estimate the Curie Temperature by means of a TGA Q500 thermogravimetric analyzer in the presence of a magnetic field at a heating rate of 10 K/min under a constant argon flow of 100 mL/min. In this method, when the sample is placed in the crucible, the apparent weight W of the sample represents the weight due to the contribution of gravity and magnetic force. Once the heating of the sample starts, changes in the measured weight could be observed, in this work, as the temperature approaches the Curie point, the apparent weight decreases. Thus, TGA in the presence of a magnetic field is a technique by which ferromagnetic events involving phase transformations and precipitation of secondary phases can be detected [34].

Based on the DSC results, the obtained ribbons samples were annealed at different temperatures to evaluate the structural evolution during heating. The annealing between the two crystallization events was considered to precipitate only the α -Fe(Si) phase, avoiding the appearance of secondary phases and to evaluate the structure, morphology and magnetic properties of the resulting structure, expecting a distribution of nanocrystalline grains in an amorphous matrix with a soft magnetic behavior. Isothermal annealing was carried out in a furnace under an argon flux of 100 mL/min for 1800s into a quartz tube. Samples were introduced in the preheated furnace at the annealing temperature. Temperature rise time is not considered.

Magnetization Vs Applied Field (M vs H) hysteresis loops were recorded with a vibrating sample magnetometer (VSM) Versalab of Quantum design at 300 K between -20 kOe and 20 kOe.

Acknowledgments

Thanks to the Ministry of Science, Technology and Innovation for the support received through its call 891 of 2020, mechanism 2, and to the Pedagogical and Technological University of Colombia—UPTC for its administrative support and the administration of resources. Special thanks are given to M.Sc. Indry Saavedra for her cooperation and technical assistance.

Author contributions

DP-C: Experimental work, analysis of the results, writing of the manuscript. CAPV.: Supervision and revision of the manuscript. FJBO.: Discussion, analysis of results and revision of the manuscript. FEE.: Discussion, analysis of results and revision of the manuscript. All authors have read and agreed to the published version of the manuscript.

Funding

Open Access funding provided by Colombia Consortium.

Data availability

The corresponding author can provide the data from the paper upon reasonable request.

Declarations

Conflict of interest The authors declare that they have no known conflicts of interests.

Open Access

This article is licensed under a Creative Commons Attribution 4.0 International License, which permits use, sharing, adaptation, distribution and reproduction in any medium or format,

as long as you give appropriate credit to the original author(s) and the source, provide a link to the Creative Commons licence, and indicate if changes were made. The images or other third party material in this article are included in the article's Creative Commons licence, unless indicated otherwise in a credit line to the material. If material is not included in the article's Creative Commons licence and your intended use is not permitted by statutory regulation or exceeds the permitted use, you will need to obtain permission directly from the copyright holder. To view a copy of this licence, visit <http://creativecommons.org/licenses/by/4.0/>.

References

1. R. Hasegawa, *Mater. Sci. Eng., A* **375–377**, 90 (2004)
2. Y. Yoshizawa, S. Oguma, K. Yamauchi, *J. Appl. Phys.* **64**, 6044 (1988)
3. Y. Yoshizawa, K. Yamauchi, *Mater. Trans. JIM* **31**, 307 (1990)
4. G. Herzer, *IEEE Trans. Magn.* **26**, 1397 (1990)
5. G. Herzer, in *Chapter 3: Nanocrystalline soft magnetic alloys*, ed. by K.H.J. Buschow. Handbook of Magnetic Materials, (Elsevier, 1997), pp. 415–462
6. K. Suzuki, A. Makino, N. Kataoka, A. Inoue, T. Masumoto, *Mater. Trans. JIM* **32**, 93 (1991)
7. M.A. Willard, M. Huang, D.E. Laughlin, M.E. Mchenry, *J. Appl. Phys.* **85**, 4421 (1999)
8. A. Inoue, B. Shen, *Mater. Sci. Eng., A* **375–377**, 302 (2004)
9. A. Makino, H. Men, K. Yubuta, T. Kubota, *J. Appl. Phys.* **105**, 1 (2009)
10. A. Inoue, R.E. Park, *Mater. Trans. JIM* **37**, 1715 (1996)
11. A. Makino, T. Kubota, C. Chang, M. Makabe, A. Inoue, *Mater. Trans.* **48**, 3024 (2007)
12. A. Makino, T. Kubota, C. Chang, M. Makabe, A. Inoue, *J. Magn. Magn. Mater.* **320**, 2499 (2008)
13. A. Makino, T. Kubota, M. Makabe, C.T. Chang, A. Inoue, *Mater. Sci. Eng. B Solid State Mater. Adv. Technol.* **148**, 166 (2008)
14. T. Kubota, A. Makino, A. Inoue, *J. Alloys Compd.* **509**, S416 (2011)
15. X. Li, A. Makino, K. Yubuta, H. Kato, A. Inoue, *Mater. Trans.* **50**, 1286 (2009)
16. A. Makino, X. Li, K. Yubuta, C. Chang, T. Kubota, A. Inoue, *Scr. Mater.* **60**, 277 (2009)
17. L. Cui, H. Men, A. Makino, T. Kubota, K. Yubuta, M. Qi, A. Inoue, *Mater. Trans.* **50**, 2515 (2009)
18. A. Makino, H. Men, T. Kubota, K. Yubuta, A. Inoue, *Mater. Trans.* **50**, 204 (2009)
19. A. Wang, C. Zhao, A. He, H. Men, C. Chang, X. Wang, *J. Alloys Compd.* **656**, 729 (2016)
20. L. Shi, K. Yao, *Mater. Des.* **189**, 108511 (2020)
21. H.S. Chen, *Rep. Prog. Phys.* **43**, 353 (2000)

22. C.W. Bale, E. Bélisle, P. Chartrand, S.A. Decterov, G. Eriksson, A.E. Gheribi, K. Hack, I.-H. Jung, Y.-B. Kang, J. Melançon, A.D. Pelton, S. Petersen, C. Robelin, J. Sangster, P. Spencer, M.-A. van Ende, *Calphad* **54**, 35 (2016)
23. H. Gao, R. Xiang, S. Zhou, B. Dong, Y. Wang, *J. Mater. Sci.: Mater. Electron.* **26**, 7804 (2015)
24. A. Inoue, *Mater. Trans. JIM* **36**, 866 (1995)
25. F.R. de Boer, W.C.M. Mattens, R. Boom, A.R. Miedema, A.K. Niessen, *Cohesion in metals: transition metal alloys* (North-Holland, Amsterdam, 1988)
26. A. Takeuchi, A. Inoue, *Mater. Trans.* **46**, 2817 (2005)
27. D.M. Minić, V.A. Blagojević, B. David, N. Pizúrová, T. Žák, D.M. Minić, *Intermetallics (Barking)* **25**, 75 (2012)
28. N. Decristofaro, A. Freilich, G. Fish, *J. Mater. Sci.* **17**, 2365 (1982)
29. H.E. Kissinger, *J. Res. Natl. Bur. Stand.* **57**, 217 (1956)
30. H.E. Kissinger, *Anal. Chem.* **29**, 1702 (1957)
31. A.H. Taghvaei, M. Stoica, K. Song, K. Janghorban, J. Eckert, *J. Alloys Compd.* **605**, 199 (2014)
32. J. Vázquez, R.A. Ligeró, P. Villares, R. Jiménez-Garay, *Thermochim. Acta* **157**, 181 (1990)
33. A. Wang, C. Zhao, H. Men, A. He, C. Chang, X. Wang, R.W. Li, *J. Alloys Compd.* **630**, 209 (2015)
34. Y. Zhou, P. Nash, *J. Alloys Compd.* **779**, 566 (2019)

Publisher's Note Springer Nature remains neutral with regard to jurisdictional claims in published maps and institutional affiliations.